Ab initio molecular dynamics study of interactions between isolated polyhedral oligomeric silsesquioxane trisilanol molecule and aluminum atoms

Deep Choudhuri a* and Andre Lee b

^a Department of Materials and Metallurgical Engineering, New Mexico Tech, Socorro, NM 87801

^b Department of Chemical Engineering and Materials Science, Michigan State University, East Lansing, MI, 48824

*Corresponding author: <u>deep.choudhuri@nmt.edu</u>

Abstract

Trisilanol polyhedral oligomeric silsesquioxane (POSS) are a category of inorganic-organic materials that comprise an inorganic open cage silica structure, organic attachments, and silanol (-Si-OH) groups. Recently, trisilanol POSS was added to Al-based alloys, and found to promote substantial microstructural refinement that improved mechanical strength and fatigue life compared to conventional Al-alloys. Such microstructural modifications and property enhancements are usually attributed to silanol-Al bonds that formed within the liquid-state prior to solidification. However, details of such high-temperature chemical interactions remain unclear. Here, we performed *ab initio* molecular dynamics simulations at 1500K, to probe the chemical interactions between isolated trisilanol POSS molecule and discreet Al atoms. Al atoms modified the silanol groups to form, two energetically favorable coordinate complexes: monodentate –Si-O-Al and bidentate –(Si-O)₂-Al. Such complexes were formed by Al atoms attracting electrons towards themselves from the POSS molecule. Crucially, this bond formation mechanism allowed POSS trisilanols to organize the neighboring Al atoms into geometric motifs that can potentially serve as nucleation sites within liquid-Al, and facilitate microstructural refinement.

1. Introduction

Nanostructured polyhedral oligomeric silsesquioxane (POSS) is a class of organosilicon compound that adopt can a cage-like structure with inorganic Si-O-Si linkages, and organic moieties (R) covalently attached to the Si vertices [1–4]. Typically, these structures are represented by the chemical formula (RSiO_{1.5})_n [1–4]. POSS-based structures show high thermal stability because of the inorganic cage or core, and can be functionalized using a variety of organic groups [1–4]. These properties permit POSS-based nanostructures to incorporated as fillers in high-temperature polymer nanocomposites, zeolites mimics, protective coatings for low earth orbit applications, and end-cappers for preventing aggregation of organic polymers in organic light-emitting diodes [1–6].

In the last decade, POSS was incorporated into metallic alloys in liquid state, and the assolidified microstructures favorably responded to mechanical and electrical stimuli [7–12]. For example, POSS additions to Sn-based solder alloys improved their strength, ability to withstand thermomechanical fatigue, and resistance to damage from electromigration [7,9–11]. These improvements were achieved by adding a category of incompletely condensed POSS that contained silanol (-Si-OH) functionality at the open vertices. One such hybrid inorganic-organic chemicals are synthesized by removing one Si atom from the vertex and protonating the exposed oxygen atoms to form three silanol groups, i.e., (R)7–O9Si7–(OH)3, – also called trisilanol POSS [1,3,4]. It is believed these silanol groups react with metal atoms in the molten state, and pin grain boundary and inter-phase interfaces in the as-solidified microstructure. Such microstructural enhancements were found to prevent performance deterioration under service conditions [7–9]. Based on this notion, phenyl trisilanol POSS, (C6H5)7–O9Si7–(OH)3, was recently added to Al-Si-Mn-Mg alloys. This addition caused microstructural refinement, and improved the tensile strength, and high-cycle fatigue life compared to conventional Al-alloys [12].

Since Al-based alloys are ubiquitous and critical for many structural applications, it is imperative to understand how the cage-bound silanols chemically interact with Al in the molten state. It is now known that Al-alloys manifest short-range ordering in liquid state by forming geometric structures or motifs that act as nucleation sites, and produce microstructural refinement [13–19]. However, most studies focus on elemental additions to Al-alloys, and fundamental studies on reactive compound additions, like trisilanol POSS, are minimal [12]. They are primarily limited by the size scale of trisilanol POSS (effective diameter ~1.4 nm), which prevents the

detection of TSP-metal bonds within metal-matrix via post-mortem characterization tools like transmission electron microscopy [12]. Such bonds are hypothesized to form via chemical reaction between liquid-Al and silanol (-Si-OH) groups, and are expected to inform the formation of the geometrical motifs within the liquid phase.

Towards that end, we have employed *ab initio* molecular dynamics (AIMD), because it can capture atomistic description of chemical reactions at desired temperatures [17,18]. Here, we have modelled the interaction between an isolated trisilanol POSS (TSP) molecule and discrete Al atoms. This simplified approach avoided perturbations introduced by the random movement of atoms in liquid phase, and close monitoring of atomistic interactions between Al and -Si-OH groups attached to the TSP cage. AIMD simulations were performed at 1500 K, which is substantially higher than the melting point of aluminum alloys. Past AIMD studies on liquid Alalloys have demonstrated that Al-based geometric motifs can form even at such high temperatures [17,18]. Therefore, AIMD simulations can provide vital structural and mechanistic insights into Al-TSP interactions at 1500 K.

2. Computational Methods

Simulations were performed using the Vienna Ab Initio Simulation Package (VASP), which employs projector augmented plane-wave (PAW) method and allows the description of the electron exchange correlation functional through generalized gradient approximation (GGA) using Perdew-Burke-Ernzerhof (PBE) parameterization [20–23]. Electronic degrees of freedom were computed by using 560 eV plane-wave cut-off energy, Γ-centered mesh using 0.2 Å-1 K-spacing for sampling the Brillouin zone, and, tetrahedron method with Blochl corrections described partial occupancies by using 0.04 eV smearing width. Long-range van der Waals interactions were incorporated using the DFT-D2 method developed by Gimme [24,25]. Our simulations employed two trisilanol POSS (TSP) molecules: (C₄H₉)₇–O₉Si₇–(OH)₃ or iso-Butyl TSP (*i*But-TSP), and (C₆H₅)₇-O₁₀Si₇-(OH)₃ or phenyl TSP (ph-TSP), since they were employed in previous studies [7,9–12]. The POSS molecules were placed inside a vacuum, by positioning them at the center of a 24×24×24 ų simulation box. This setup was energy minimized with respect to ionic and electronic degrees of freedom till the Hellman-Feynman forces were less than ~1 meV/Å. The optimized geometries – corresponding to 0 K – were further equilibrated at 1500 K for 1ps using ab initio molecular dynamics (AIMD). These simulations employed canonical (NVT) ensemble, where the equations of motion were integrated using 1 fs time step. Temperature was controlled

via Andersen thermostat, which uses collision frequency ν , i.e., coupling strength between temperature bath and system, to achieve a desired temperature [26]. Systematic testing indicated that ν =0.01-0.05 gave consistent results. However, ν =0.05 was employed to carry out all production runs, because it permitted computational efficiency. This value is consistent with literature reports [26–29]: they prescribe smaller ν values, because that minimizes alteration of phase-space trajectories from stochastic collisions. The interaction of silanol (Si-OH) bonds with aluminum (Al) was interrogated by placing one-, two- and three-Al atoms near the free Si-OH bonds in three separate supercells of each TSP molecule. Subsequently, NVT-AIMD was performed at 1500 K for 5 ps, where temperature and energy equilibration was achieved within 0.5 ps..

Simulation results were analyzed by interrogating the equilibrated structures, lattice dynamics and energetics of Al-TSP interactions. Molecular structures were visualized using VESTA and atomic trajectories were computed via OVITO packages [30,31]. Interatomic distances and structural ordering were characterized by computing pair correlation or partial radial distribution functions (PDF) using the relationship [17,26]:

$$g_{\alpha\beta}(r) = \frac{1}{N_{\alpha}N_{\beta}} \sum_{i=1}^{N_{\alpha}} \sum_{j=1}^{N_{\beta}} \langle \delta(\left|\vec{r}_{i} - \vec{r}_{j}\right| - r_{shell}) \rangle \tag{1}$$

where, N_{α} and N_{β} are the no. of α and β -type atoms, respectively, $|\vec{r}_i - \vec{r}_j|$ is the distance between α and β atoms, r_{shell} is the distance of the shell from a central atom, and δ is the delta function. In this study, we have focused on C-H and C-C PDFs, because they allowed us to distinguish between iso-butyl and phenyl moieties in the TSP. Furthermore, PDFs were computed by averaging over several time-steps after achieving equilibration.

Lattice dynamics at 1500 K was probed by calculating the velocity autocorrelation function (VAF) and, subsequently, converting VAF to frequency domain using Fourier transform [26,32]. This transformation into frequency domain allowed us to extract the phonon density of states of structures at 1500 K [32]. VAF was first computed using:

$$C(t) = \frac{1}{NM} \sum_{j=1}^{N} \sum_{m=1}^{M} v_j(m \times \Delta t). v_j(m \times \Delta t + t)$$
 (2)

where, C(t) is the correlation function, t is time, N total no. of atoms, M total number of steps, and Δt time step used in the AIMD simulations. Subsequent conversion to the frequency domain (ω) was performed via the Fourier transform,

$$Z(\omega) = \int_{-\infty}^{\infty} C(t)e^{-i\omega t}dt$$
 (3).

where, $Z(\omega)$ is the vibrational spectra representing phonon density of states (PDOS) [32]. Equations (1)-(3) were applied by conservatively sampling the last 1000 steps (i.e., from 4-5 ps) for each AIMD simulation, because it allowed us to probe structural variations after equilibration. Finally, the per-atom interaction energy of Al with TSP was estimated using the expression:

$$\langle \Delta E_i \rangle = \frac{\langle \mathcal{H}(POSS-Si-O-Al) \rangle - \langle \mathcal{H}(POSS-Si-OH) \rangle - N_{Al} \times \langle \mathcal{H}(N_{Al}^{vac}) \rangle}{N_{Al}} \tag{4}$$

Where, $\langle \Delta E_i \rangle$ is the per-atom interaction energy, and, $\langle \mathcal{H}(POSS-Si-O-Al) \rangle$ and $\langle \mathcal{H}(POSS-Si-OH) \rangle$ are the system Hamiltonians after reacting with N_{Al} -Al atoms, and of pristine molecule at 1500 K, respectively. $\langle \mathcal{H}(N_{Al}^{vac}) \rangle$ is the per-atom Hamiltonian of N_{Al}^{vac} Al atoms. This configuration was placed in the vacuum of a simulation box with dimensions $25 \times 25 \times 25 \text{ Å}^3$ and equilibrated at 1500 K for 2 ps. $\langle \mathcal{H}(N_{Al}^{vac}) \rangle$ was computed by using $N_{Al}^{vac} = 20$, 50 and 100, and an average energy value was used as an input in eq.4. Additionally, the $\langle ... \rangle$ in eq.4 indicates values averaged over the last 1ps after achieving temperature equilibration. Thus, we have computed $\langle \Delta E_i \rangle$ for *i*But-TSP and *ph*-TSP after reaction with one (1)-, two (2)- and three (3)-Al atoms.

3. Results and Analysis

First, we examined pristine TSPs to understand the effect of organic moieties on the equilibrium structures of *i*But-TSP and *ph*-TSP at 1500 K. Fig.1a1 and 1b1 show AIMD snapshots at 1ps of *i*But-TSP and *ph*-TSP, respectively. Since these structures were obtained after equilibration, they demonstrate the high-temperature structural stability of the inner Si-O-Si cage (-O₁₂Si₇-). In Fig.1a1 and 1b1, the hydroxyl bonds are attached to the corner Si atoms to form silanol (-Si-OH) groups (marked using ellipses). These Si atoms are marked as Si1, Si2 and Si3 in Fig.1a1 and 1b1. The organic moieties, attached to the corner Si atoms in the Si-O-Si cage, were characterized by computing the time-averaged PDFs of the constituent C–H (Fig.1a2 and 1b2) and C–C bonds (Fig.1a3 and 1b3). These 1500 K PDFs were also compared with the energy minimized structures corresponding to 0 K (shaded peaks in Fig.1a2, 1b2, 1a3 and 1b3). The 0 K-PDFs contained distinct peaks corresponding to 1st, 2nd, 3rd, and 4th nearest-neighbors (NN), which is indicative of long-range order or crystalline periodicity within the isolated, energy-minimized TSP molecules [1,3]. It is worth noting that room-temperature crystallinity has been reported in bulk *i*But-TSP and *ph*-TSP [33–35]. Thus, our 0 K DFT results are consistent with such experimental observations. Next, we examine the PDF peaks corresponding to 1500 K.

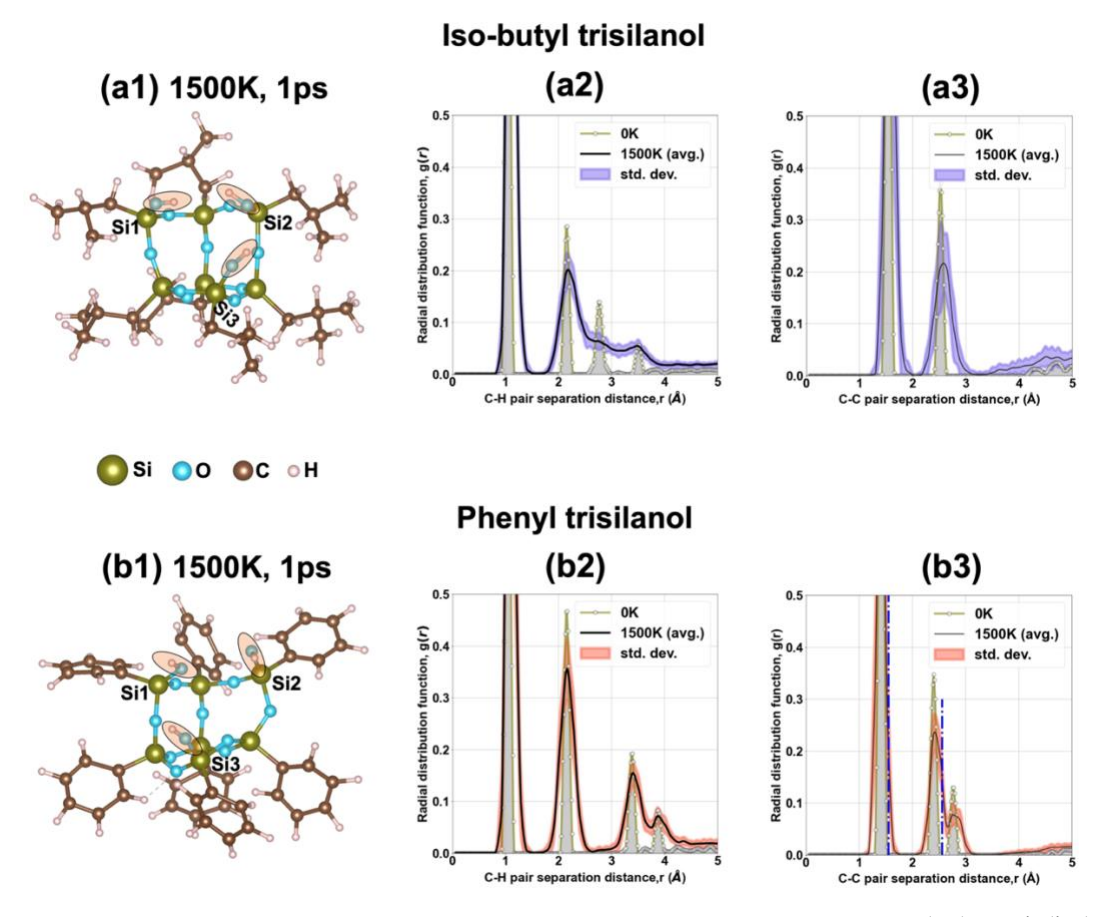


Figure.1. Structures of isolated POSS trisilanols molecules at 1500 K. (a1) and (b1) show AIMD snapshots of isobutyl and phenyl POSS at 1ps, respectively. (a2) and (b2) are the corresponding time-averaged partial PDFs of C-H bonds in the iso-butyl and phenyl moieties, respectively, while (a3) and (b3) show their time-averaged partial PDFs corresponding to C-C bonds. All PDFs were averaged by using snapshots within 0.5-1 ps: bold line indicates the average value and spread is the standard deviation. Corresponding PDFs at 0 K are also shown in (a2)-(b3). In (b3), the dash-dot lines are the 1st and 2nd nearest-neighbor peak locations of iso-butyl trisilanol POSS.

Fig.1a2 and 1b2 shows that equilibration at 1500 K retained the 1st and 2nd NN peaks in both TSPs, but manifested convoluted higher-order NN peaks (in comparison to 0 K). Such convolution indicated a reduction in the long-range order of the TSP structure, possibly due to thermal vibrations at 1500 K. Furthermore, such vibrational modes will be influenced by the type of moieties, i.e., iso-butyl (C₄H₉–) v.s. phenyl (C₆H₅–), because they have different molecular weights [32]. A phenyl group has higher molecular weight than the iso-Butyl group, which is expected to impart vibrational movement of bonds to a lesser degree in the phenyl group [32], e.g.

compare insets in Fig.2a and 2b. This effect is readily noted in the 3rd NN peaks of *ph*-TSP and *i*But-TSP (Fig.1a2 and 1b2), where the former manifested relatively sharper 3rd NN peak.

To better understand the differing vibrational tendencies of iso-butyl and phenyl groups, we have computed the phonon density of states (PDOS) of *both* TSPs using eqs. (2) and (3). Fig.2a and 2b plots PDOS v.s. frequency (ω) of *i*But-TSP and *ph*-TSP at 1500 K, respectively. The vertical lines in these plots indicate stretching vibrational frequencies obtained from literature reports, where bulk *i*But-TSP and *ph*-TSP specimens were examined using FTIR [33–35]. For example, the gray lines correspond to stretching frequencies of Si-O-Si bonds present in the inorganic silica cage: 831 and 1086 cm⁻¹ for *i*But-TSP [33], and 1000 and 1300 cm⁻¹ for *ph*-TSP [34,35]. The colored lines in Fig.2a (blue color) and 2b (red color) show frequencies corresponding to the C-H bonds within the organic moieties: 1328, 1366, 1400, 1463, 2868, 2900 and 2950 cm⁻¹ for *i*But-TSP [33], and 678, 740, 1492, 1510, 1430, 1641, 3003 and 3093 cm⁻¹ for *ph*-TSP [34,35]. Comparison with such experimental stretching frequencies provided an approximate approach for interpreting our AIMD-based PDOS spectra (Fig.2), because it is difficult to measure such frequencies for an isolated, nanoscale TSP molecule.

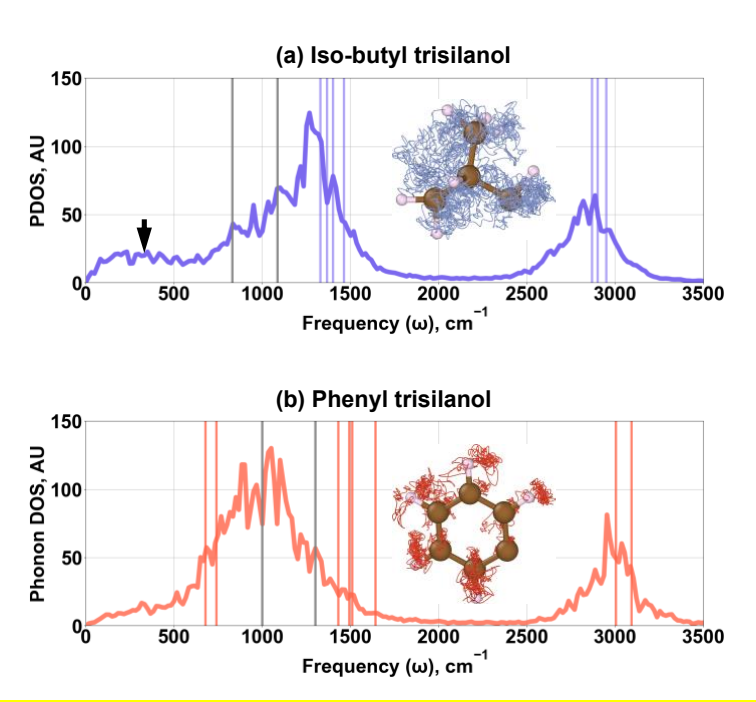


Figure.2. Vibrational spectra obtained from AIMD at 1500 K: Plots comparing phonon density of states vs. frequency of isolated (a) iso-butyl and (b) phenyl trisilanol POSS. Insets show the trajectories of C and H atoms in a selected (a) iso-butyl and (b) phenyl moiety within 4-5ps. Brown and pink colored atoms are C and H, respectively.

A detailed analysis of the vibrational spectra indicated that the C-H bonds in *i*But-TSP manifested higher PDOS compared to ph-TSP within the range ~1300-1500 cm⁻¹. In Fig.2, this range was located near the maxima (Fig.2a) and tail-end (Fig.2b) of the first peak of iBut-TSP and ph-TSP spectra, respectively; meaning, frequencies within the range ~1300-1500 cm⁻¹ will significantly impact on the structure of iBut-TSP. Notionally, C-H vibrations will be influenced by the stretching and torsional movement of the underlying carbon-carbon skeletal framework. The sp³ hybridized C-C single bonds in iso-Butyl are structurally more flexible than sp² hybridized C=C double bonds in the phenyl group, because the former can easily undergo both stretching and torsional movement compared to the latter [36]. The π -bonds in C=C tend to restraint torsional movements [36]. The effect of single vs. double bonds on the vibrational movement of moieties is demonstrated in the insets of Fig.2a and 2b, which shows the trajectories of C and H atoms of a representative iso-Butyl and phenyl group, respectively. The iso-Butyl group experienced substantially greater movement compared to phenyl. Therefore, the vibrations of C-H bonds are better accommodated by the "flexible" C-C skeletal structure of iso-Butyl moieties by manifesting higher PDOS within ~1300-1500 cm⁻¹. Consequently, iBut-TSP experienced reduced long-range order at 1500 K, and such structural change is manifested as convoluted higher-order NN peaks in the C-H PDFs (compare Fig. 1a2 and 1b2).

Crucially, our AIMD results demonstrate that isolated iso-butyl and phenyl POSS trisilanol molecules are structurally stable at 1500K; albeit with reduced long-range order compared to 0 K. Subsequently, these *i*But-TSP and *ph*-TSP structures were used as starter structures for examining interactions with Al atoms. This permitted us to probe the effect of relative flexible iso-Butyl and rigid phenyl moieties on the chemical reactivity of three silanol groups with Al atoms. (Hereafter, the terms interaction and reaction are used interchangeably).

Panels in Fig.3a and 3b compare and contrast reaction products at 1500 K, after *i*But-TSP and *ph*-TSP interacted with one- (panels 3a1-3b1), two- (panels 3a2-3b2), and three- (panels 3a3-3b3) Al atoms. Each panel show AIMD snapshots at 5 ps. Fig.4 separately shows Si-O-Al bonds, after reaction with one- (Fig.4a), two- (Fig.4b), and three- (Fig.4c and 4d) Al atoms, by extracting the reactive part from the TSP molecule. Since the reaction with one and two- Al atom formed the same type of Si-O-Al bonds for both *i*But-TSP and *ph*-TSP, we have shown the results for *i*But-TSP in Fig.4a and Fig.4b, only.

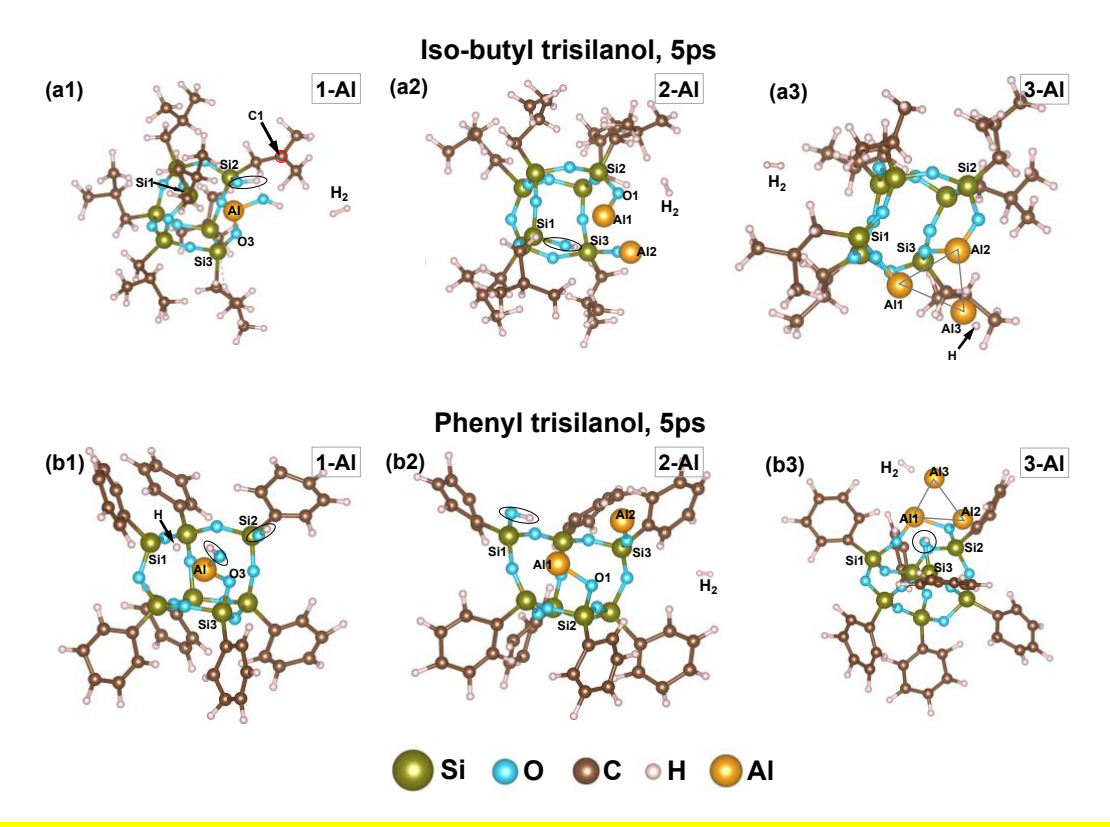


Figure.3. Interaction of isolated iso-butyl and phenyl trisilanol POSS molecules with Al atoms. AIMD snapshots at 5 ps depicting simulations results using (a1)-(b1) one, (a2)-(b2) two, and (a3)-(b3) three Al atoms.

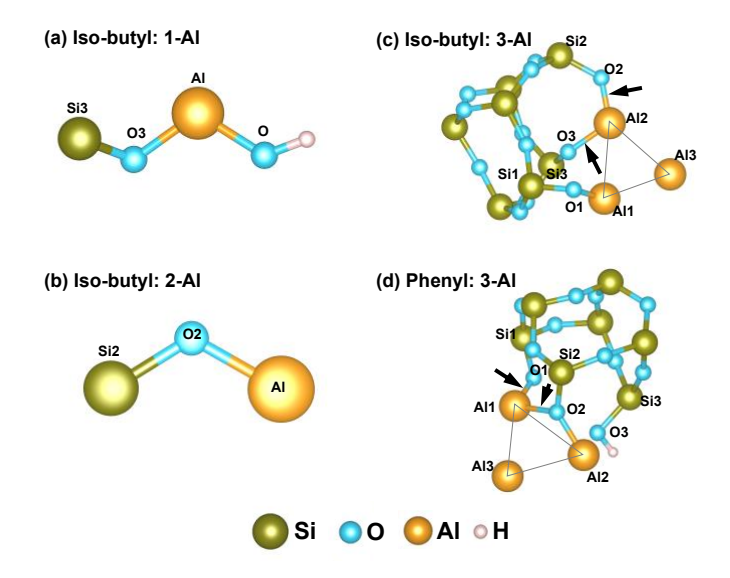


Figure.4. Representative reaction products. Interaction of silanol with (a) one-Al formed monodentate Si-O-Al-OH, (b) two-Al formed monodentate Si-O-Al, and (c)-(d) three-Al formed bidentate Si-O-Al.

Fig.3a1 and 3b1 show that reaction with single Al formed a dangling, monodentate -Si-O-Al-OH group in the two TSP variants. This reaction product is separately shown in Fig.4a. The key difference between the two interactions (i.e., Fig.3a1-3b1) is that the reaction with *i*But-TSP released a hydrogen molecule (H₂), but not for *ph*-TSP. In the case of *i*But-TSP, a H atom, associated with either Si1 or Si3, reacted with another H attached to one of the carbon atoms in the iso-butyl group (marked as C1). This left a lone Si atom (Si1) that was without any attachments (marked with an arrow in Fig.3a1). In contrast, H atoms in *ph*-TSP were bound to the phenyl groups and a Si atom (Si1). The Si1 lost an oxygen atom from its OH group, but retained one H atom in its proximity. Notwithstanding, in both TSPs, reactions with single Al affected two silanol groups, but left only one silanol group unchanged, i.e., Si2-OH (marked with a shaded ellipse). Taken together, these single atom simulations reveal the chemical affinity of Al atom towards silanol groups, and that additional interactions, e.g., release of hydrogen molecule, appears to be influenced by the type of organic moieties, i.e., iso-butyl vs. phenyl groups.

Interestingly, the difference in organic moieties had minimal impact on the chemical reactivity of *i*But-TSP and *ph*-TSP with two Al atoms (Fig.3a2 and 3b2). Both TSPs manifested comparable interactions. The Al atoms reacted with two silanol groups to form two monodentate -Si-O-Al (e.g., see Fig.4b). The reaction with each silanol group yielded two H atoms that combined to form H₂. Again, this reaction left one unaltered silanol, i.e., Si1-OH- see shaded ellipses in Fig.3a2 and 3b3. It is worth pointing out that the reaction of two Al atoms differed significantly from the one-Al atom interactions, which formed a -Si-O-Al-OH group (compare Fig.4a and 4b). Broadly, we find that Si-O-Al formation was facilitated by increasing Al content, where Al atoms displace hydrogen in Si-OH groups.

The trend of replacing H atoms, and releasing a H₂ molecule, continued with three-Al interactions (Fig.3a3 and 3b3), but there were major differences with two-Al atom interactions (Fig.3a2 and 3b2). The interaction with three-Al formed bidentate coordinate complex, which are indicated with arrows in Fig.4c and 4d for *i*But-TSP and *ph*-TSP, respectively. These bidentate bonds comprised of an Al atom connected to two -Si-O-, i.e., Si3-O3-Al2-O2-Si2 and Si1-O2-Al1-O2-Si2 in *i*But-TSP and *ph*-TSP, respectively. Monodentate Si-O-Al complexes also formed after interacting with three Al atoms, e.g., Si1-O1-Al1 in *i*But-TSP (Fig.4c). Interestingly, one "unattached" Al atom was noted in both cases that did not interact with any of the silanol groups (marked Al3 in Fig.4c and 4d). Importantly, we find that the bi- and mono-dentate Al atoms, and

the unattached-Al3 formed stable triangular motifs at 1500 K. These structures are schematically indicated using triangles in Fig.4c and 4d. Significance of such geometric motifs will be discussed later.

Comparison of Fig.4c and 4d also revealed the influence of iso-butyl and phenyl group. All three Si-OH groups in *i*But-TSP were involved in the reaction, while only two Si-OH participated in *ph*-TSP. The unreacted silanol group is indicated by Si3-O3-H in Fig.4d. Furthermore, interaction with three Al with *i*But-TSP replaced three H atoms, and yielded an excess H that remained bound to Al3 (indicated with an arrow in Fig.3a3). Taken together, we learn that increasing Al content from one to three atoms modifies the –Si-OH silanol bonds in the following order: –Si-O-Al-OH (one-Al interaction), –Si-O-Al (two-Al interaction), and bidentate –(Si-O)₂-Al (two- and three-Al interaction).

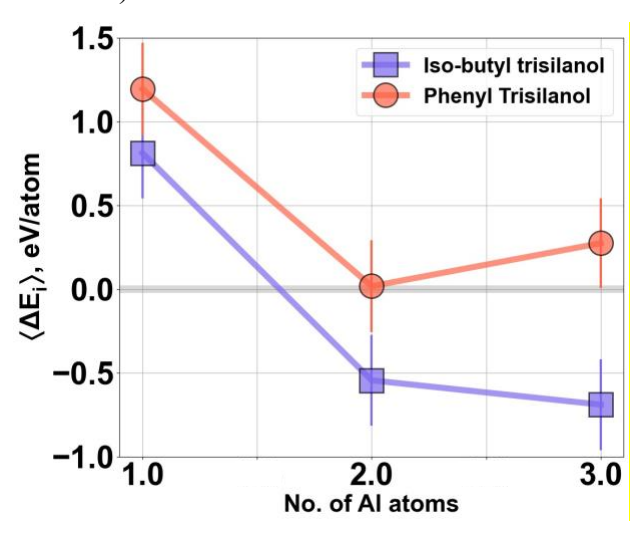


Figure.5. Energetics of Al-TSP interaction. Plots comparing interaction energies as function of Al atoms for *i*But-TSP and *ph*-TSP.

Next, we quantified the effect of the number of Al and type of moieties by computing peratom interaction energy ($\langle \Delta E_i \rangle$) using eq.3. These results are presented in Fig.5, and they compare $\langle \Delta E_i \rangle$ v.s. no. of Al atoms (N_{Al}) plots for both *i*But-TSP and *ph*-TSP. Broadly, they show that $\langle \Delta E_i \rangle$ reduces with increasing N_{Al} , which implied that the formation of bidentate –(Si-O)₂-Al and monodentate –Si-O-Al bonds are energetically more favorable than–Si-O-Al-OH, and, by extension, formation of triangular motifs (depicted in Fig.4c and 4d). These plots also showed that interaction of Al with isolated *i*But-TSP is energetically more favorable than that of *ph*-TSP, and underscores the effect of iso-butyl and phenyl moieties on silanol-Al interactions. The remaining

sections will focus on TPSs that reacted with three-Al atoms, because they formed geometric motifs that relevant to nucleation in Al-based alloys [13–17,19] (also see *Section.4*).

The influence of moieties on TSP structure was further probed by examining their timeaveraged PDFs of C-H (Fig.6a) and C-C (Fig.6b) bonds. The C-H PDFs for both structures had comparable 1st and 2nd NN peak locations (Fig.6a). This suggested that the H atoms are tightly bound to the neighboring carbon atoms in both moieties, and are able to move in tandem with them at 1500 K. We also note that both mojeties manifested convoluted higher-order NN peaks in their C-H PDFs, with phenyl showing shaper peaks than iso-Butyl groups. These results are comparable to the pristine molecules (see Fig.1), and indicated minimal influence of Al atoms on the longrange order in isolated TSPs. Interestingly, the peak locations in C-C PDFs of iBut-TSP were shifted to the right compared to ph-TSP; meaning, the C-C bond lengths in iBut-TSP were greater than ph-TSP (Fig.6b). This feature was also noted in C-C PDFs of pristine molecules, and such peak shifts are indicated with vertical dotted lines in Fig. 1b3. The longer bond length point towards the underlying flexible skeletal C-C bonds in iso-butyl groups, and is consistent with higher vibrational PDOS seen in the pristine structure (see Fig.2). This structural feature afforded iso-butyl groups with a greater degree of vibrational freedom compared to the phenyl attachments, and possibly allowed better accommodation of the interacting Al atoms. Notwithstanding, these observations indicated that the structure of TSPs, after reacting with 3 Al atoms at 1500 K, were largely comparable to the pristine structures (see Fig. 1a2, 1a3, 1b2 and 1b3).

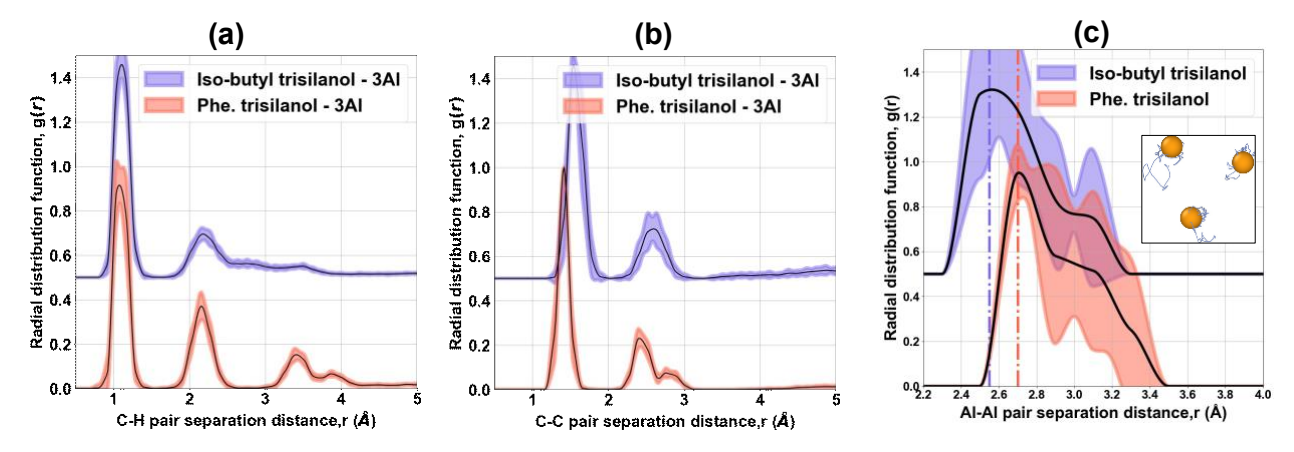


Figure.6. Comparison of structures after annealing at 1500 K. Plots showing time-averaged partial PDFs of (b) C-H and (c) C-C bonds in organic moieties of POSS after reacting with three-Al atoms at 1500 K. (c) compares pair-separation distances between Al atoms within the triangular

motifs. Inset in (c) shows the trajectories of 3Al atoms in *iBut*-TSP. Averaging was performed within 4-5 ps, and the bold lines indicate average values.

Next, we examined the effect of iso-Butyl and phenyl moieties on the triangular motifs formed by three Al atoms (see Fig.4c and 4d). Towards that end, time-averaged Al-Al PDF was computed and plotted in Fig.6c. The distribution in these plots indicated that the triangular geometry was largely persistent after equilibration; despite thermal vibrations resulting from annealing at 1500 K (e.g., see inset). The influence of moieties was discerned from the pairseparation corresponding to 1st NN peaks (indicated with vertical lines in Fig.6c). The average Al-Al interatomic distance in *iBut*-TSP was slightly shorter than *ph*-TSP, which is usually associated with enhanced interatomic bonding [37–39]. Such bonding can also lower the interaction within three-Al. Therefore, to better understand the bonding in the triangular motifs in *iBut*-TSP and *ph*-TSP we have performed Bader charge analysis [40–42], and computed excess electron charge distribution. Such electronic structure analysis was performed on structures obtained after 5 ps of annealing at 1500 K, and included -Si-O- bonds because they are bonded to the Al atoms comprising the triangular motifs (see Fig.4c and 4d). Recall that all three -Si-OH bonds in iBut-TSP participated in the reaction (Fig.4c), while two such bonds interacted with Al in the case of ph-TSP, with one -Si-OH remaining intact (Fig.4c). Results from Bader analysis is presented in Table I, while the spatial distribution of electronic charge density is shown in Fig.7.

Table I. Bader analysis showing per-atom charges on Si, O and Al atoms in *iBut*-TSP and *ph*-TSP that reacted with three-Al atoms. Values are in electron (e) units.

Structure	Si1-O1-Al1			Si2-O2-Al2			Si3-O3		Unattached
	Si1	01	Al1	Si2	O2	Al2	Si3	O3	Al3
iBut-TSP	3.02e b	-1.62e b	0.89e b	3.11e ^a	-1.62e a	1.43e ^a	3.01e ^a	-1.61e ^a	0.88e
ph-TSP	3.02e ^a	-1.59e ^a	1.00e ^a	2.99e a, b	-1.70e a, b	0.68e b	3.99e ^c	-1.39e ^c	2.03e

^a Forms bidentate coordinate complex

Table I shows the on-site charge of Si, O and Al atoms in *iBut*-TSP and *ph*-TSP, where positive and negative values correspond to electronic charge on-site depletion and localization. For reference, the ideal valences of Si, O and Al are +4e, -2e and +3e, respectively. Note, the atomic indices used in the analysis corresponded to those indicated in Fig.4c and 4d. A careful

^b Forms monodentate coordinate complex

^c Unreacted silanol

examination of Table I revealed four key observations. First, most on-site Bader charges listed in Table I significantly differed from the ideal valences; meaning, such atoms will have a greater tendency to form covalent bonds instead of ionic bonds [37]. For example, atoms constituting the bi- and mono-dentate Si-O-Al coordinate complexes will form covalent bonds. Second, charges on Si and O in iBut-TSP were relatively uniform compared to ph-TSP. Such uniformity in iBut-TSP, and lack thereof in ph-TSP, is presumably due to the reactivity of all three silanol groups with Al (compare Fig 4c and 4d). An extreme case of charge non-uniformity was noted in the case of Si3 that belonged to the unreacted silanol group in ph-TSP (Fig.4d). Its value was comparable to the ideal valences of +4e, which was significantly greater than Si1 and Si2 in both *iBut*-TSP and ph-TSP. Third, Al atoms forming bidentate complex had greater positive charge compared to monodentate Al, e.g., compare All and Al2 values in Table I for iBut-TSP. However, the value of bidentate Al atom in *iBut*-TSP was greater than *ph*-TSP. This difference was likely related to the non-uniformity in the charge distribution on Si and O atoms in ph-TSP. Fourth, such nonuniformity also influenced the charge depletion (positive charge values) of the unattached Al3 atom: higher values were noted in ph-TSP compared to iBut-TSP. Taken together, the relative uniformity in the charge values on the Si, O and Al atoms in iBut-TSP may have contributed to the overall stability of iBut-TSP-3Al structures, and, presumably, lowered its interaction energy with Al atoms in comparison to ph-TSP at 1500 K.

Finally, we examined the bonding character of the immediate neighborhood of the triangular motifs by computing the excess electron charge density distribution. Such densities were obtained using, $\Delta \rho_{excess} = \rho_{POSS-Si-O-Al} - \rho_{POSS-Si-O-} - \rho_{Al}$; where, $\rho_{POSS-Si-O-Al}$, $\rho_{POSS-Si-O-}$, and ρ_{Al} are charge densities of the complete molecule with Al attachments, iBut/ph-TSP-Si-O- after removing the Al atoms, and only the Al atoms (by removing the associated TSP), respectively. Structures equilibrated for 5ps were used for this purpose. Fig.7a and 7b shows the $\Delta \rho_{excess}$ surrounding iBut-TSP and ph-TSP, respectively, using yellow-colored 3D contours, and they yielded two insights. *First*, excess charge is concentrated around the Si-O bonds and attached organic moieties located next to the Al-based motifs (indicated with triangles in Fig.7a and 7b). Excess charge density was prominent noted near the Al motifs, as well. In other words, Al atoms showed a tendency to draw the electrons towards themselves; meaning, they act like Lewis acid (electron acceptors). Interestingly, organic moieties located farther from such Al atoms served as Lewis bases (electron donors), since they were depleted of excess charge (marked with ellipses).

Second, charge localization between Al-Al suggest that they are covalently bonded, which is also consisted with the Bader charge analysis (see Table I). In the past, such bonding between "classically" metallic atoms have been noted in Al-, Mg- and Ti-based alloys [17,18,38,39,43]. Crucially, these results rationalize why the triangular motifs are geometrically persistent despite being subjected to thermal vibrations at 1500 K - they are held together by strong covalent bonds.

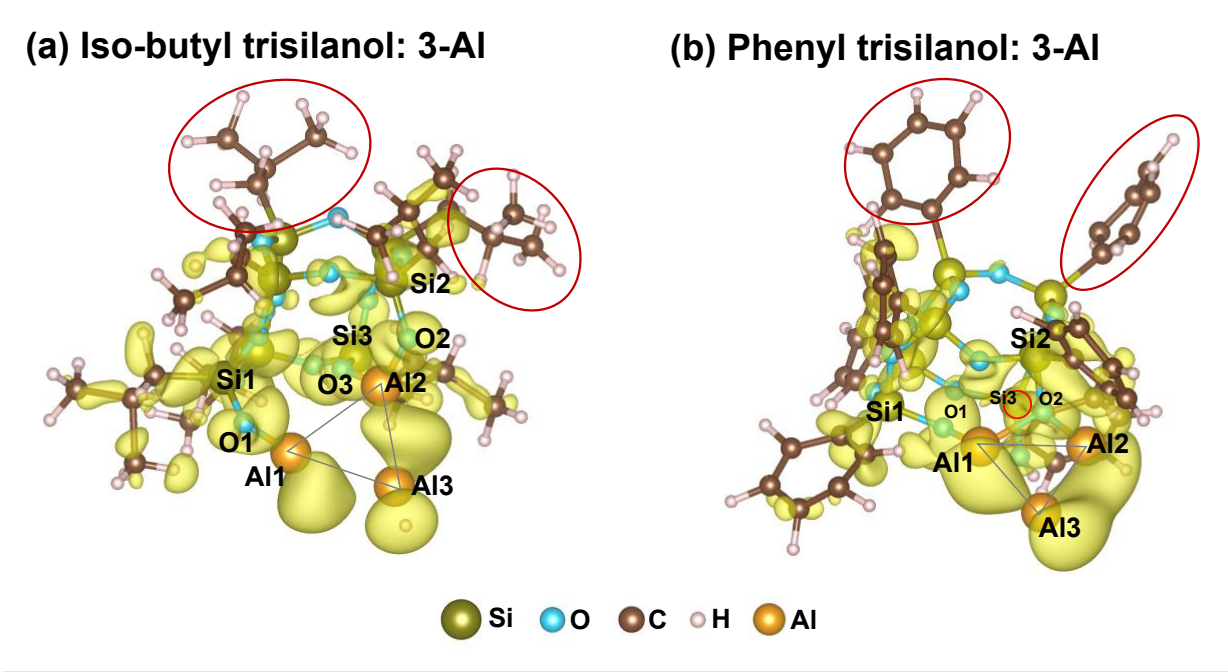


Figure.7. Comparison of excess electronic charge densities in (a) iso-Butyl and (b) phenyl trisilanol POSS structures Al-based triangular motifs.

4. Discussion

Our simulations have two important implications within the context of crystallization and energy production. The persistent triangular structures seen in Fig. 4c and 4d can be related to crystallization within molten phase. Classical mean-field studies, employing classical density functional theory and phase-field crystal-based simulations, have shown that in-liquid triangular facets act as nucleation sites [19,44,45]. Furthermore, electron-backscattered diffraction-based characterization of as-solidified microstructures of Al-Cr, Al-Zn and Al-Cr-Zn alloys suggested that triangular facets on short-ranged ordered polyhedrons, within the liquid-phase prior to crystallization, facilitated face-centered-cubic (*fcc*)-Al nucleation [13–15]. This mechanism was also corroborated in a recent study on Al-Sc alloys that utilized AIMD simulations to examine short-ranged ordering in the liquid phase [17]. They showed that triangular facets on Sc-centered polyhedrons were instrumental in nucleating the solid phase. These literature observations suggest

that the triangular motifs formed by TSP will facilitate heterogenous nucleation solid Al. Our simulations suggest that such geometric motifs will be structurally and chemically supported by forming monodentate –Si-O-Al and bidentate –(Si-O)₂-Al bonds (Fig. 4c and 4d) within liquid-Al. The net effect will be the modification and refinement of the as-solidified microstructure, which is well-documented to improve tensile and fatigue strengths; particularly after adding trisilanol POSS chemicals [46,47,12].

Broadly, we hypothesize that trisilanol POSS have a tendency to form geometrically favorable structures that can potentially act as potent sites for nucleation of *fcc*-Al within the liquid phase. These structures will comprise metal atoms that will be likely held together by a combination of mono- and bi-dentate metal-Si-O bonds "supplied" by the inorganic –O₁₂Si₇–cages. The dynamics of metal-organic moieties interaction within liquid phase, and the effect of such interactions on the structural stability of such moieties remains unclear, because the present study investigated metal-atom interactions with isolated molecules, and excludes probing interaction with liquid phase. This matter is currently under investigation.

Finally, the release of hydrogen molecules after reacting with Al atoms – see Fig.3 – suggest that trisilanol POSS may be employed for energy applications. Specifically, they can be utilized as prototypical chemicals for testing technologies for H₂-generation and storage, where the holding temperatures can be reduced by using low-meting metals like Tin (Sn). Their alloys are readily available, melt around at significantly lower temperature than Al, i.e., ~576 K, and are well-documented to interact with trisilanol POSS [7,9–11].

5. Summary

Ab initio molecular dynamics simulations were performed to examine the interaction of one-, two-three-Al atoms with the silanol (S-OH) groups attached to isolated hybrid organic-inorganic polyhedral silsesquioxane (POSS) molecules. We also examined the effect of iso-butyl and phenyl organic moieties that are attached to the corner Si atoms in POSS. Simulations were performed at 1500 K, and they provided crucial insights into high-temperature reaction mechanisms between Si-OH groups and Al. Key results from our study are as follows:

1. The reaction between Si-OH groups and one- two- and three-Al atoms resulted in –Si-O-Al-OH, –Si-O-Al, and –(Si-O)₂-Al bonds, respectively. Detailed examination of the interaction energies revealed that monodentate –Si-O-Al and bidentate –(Si-O)₂-Al were energetically more favorable than –Si-O-Al-OH. The Al atoms acted as Lewis acids

accepting electrons, while organic moieties far from those Al atoms served as Lewis bases by donating electrons. Reaction with Al atoms also releases a hydrogen molecule as a biproduct.

- 2. The reaction with three Al atoms formed Al-based triangular structures. In general, this suggested the tendency of trisilanol POSS to form Al-based geometric structures in the presence of multiple metal atoms, and such structures may serve as heterogenous nucleation sites within the liquid melt of Al-alloys.
- 3. Energetic considerations also indicated that the isolated trisilanol POSS attached to iso-Butyl groups interacted more favorably with Al atoms compared to those with phenyl groups. Possible factors contributing to such favorable interactions are: Enhanced vibrational degree of freedom of the iso-Butyl moieties; relatively uniform distribution of on-site atomic charges; and avoiding charge localization.

Acknowledgement

DC is grateful for funding from NSF-DMR#2333630 and PRF#67077-ND10. DC also acknowledges computation time on the Alpine High-Performance Computing resource at the University of Colorado Boulder. Alpine is jointly funded by the University of Colorado Boulder, the University of Colorado Anschutz, Colorado State University, and the National Science Foundation (award # 2201538).

Data Availability Statement

The data that supports the findings of this study are available within the article.

References

- [1] Phillips SH, Haddad TS, Tomczak SJ. Developments in nanoscience: polyhedral oligomeric silsesquioxane (POSS)-polymers. Curr Opin Solid State Mater Sci. 2004;8:21–29.
- [2] Liu H, Kondo S, Tanaka R, et al. A spectroscopic investigation of incompletely condensed polyhedral oligomeric silsesquioxanes (POSS-mono-ol, POSS-diol and POSS-triol): Hydrogen-bonded interaction and host–guest complex. J Organomet Chem. 2008;693:1301–1308.
- [3] Cordes DB, Lickiss PD, Rataboul F. Recent Developments in the Chemistry of Cubic Polyhedral Oligosilsesquioxanes. Chem Rev. 2010;110:2081–2173.

- [4] Zhang W, Müller AHE. Architecture, self-assembly and properties of well-defined hybrid polymers based on polyhedral oligomeric silsequioxane (POSS). Prog Polym Sci. 2013;38:1121–1162.
- [5] Kannan RY, Salacinski HJ, Butler PE, et al. Polyhedral Oligomeric Silsesquioxane Nanocomposites: The Next Generation Material for Biomedical Applications. Acc Chem Res. 2005;38:879–884.
- [6] Zhen C-G, Becker U, Kieffer J. Tuning Electronic Properties of Functionalized Polyhedral Oligomeric Silsesquioxanes: A DFT and TDDFT Study. J Phys Chem A. 2009;113:9707– 9714.
- [7] Lee A, Subramanian K, Lee J-G. Development of nanocomposite lead-free electronic solders. IEEE; 2005. p. 276–281.
- [8] Choudhuri D. Influence of nano-structured chemicals on the microstructures and mechanical reliability of lead-free tin-based solders. 2009;
- [9] Zhang R, Xu G, Wang X, et al. Electromigration in Sn-Bi Modified with Polyhedral Oligomeric Silsesquioxane. J Electron Mater. 2010;39:2513–2521.
- [10] Liu S, Ma L, Shu Y, et al. Effects of POSS-Silanol Addition on Whisker Formation in Sn-Based Pb-Free Electronic Solders. J Electron Mater. 2014;43:26–32.
- [11] Ma L, Zuo Y, Liu S, et al. Whisker growth behaviors in POSS-silanol modified Sn3.0Ag0.5Cu composite solders. J Alloys Compd. 2016;657:400–407.
- [12] Lu Y, Godlewski LA, Zindel JW, et al. Use of reactive nanostructured chemicals for refinement of Si eutectic in an aluminum casting alloy. J Mater Sci. 2019;54:12818–12832.
- [13] Kurtuldu G, Jarry P, Rappaz M. Influence of Cr on the nucleation of primary Al and formation of twinned dendrites in Al–Zn–Cr alloys: Can icosahedral solid clusters play a role? Acta Mater. 2013;61:7098–7108.
- [14] Kurtuldu G, Sicco A, Rappaz M. Icosahedral quasicrystal-enhanced nucleation of the fcc phase in liquid gold alloys. Acta Mater. 2014;70:240–248.
- [15] Kurtuldu G, Jarry P, Rappaz M. Influence of icosahedral short range order on diffusion in liquids: A study on Al-Zn-Cr alloys. Acta Mater. 2016;115:423–433.
- [16] Choudhuri D, Majumdar BS. Structural changes during crystallization and vitrification of dilute FCC-based binary alloys. Materialia. 2020;12:100816.
- [17] Choudhuri D, Majumdar BS, Wilkinson H. Investigation of in-liquid ordering mediated transformations in Al-Sc via ab initio molecular dynamics and unsupervised learning. Phys Rev Mater. 2022;6:103406.

- [18] Wilkinson H, Boyd B, O'Connell JM, et al. Factors controlling heteroepitaxial phase formation at intermetallic-Al3Sc/liquid interfaces. J Appl Phys. 2023;133:124902.
- [19] Chaikin PM, Lubensky TC, Witten TA. Principles of condensed matter physics. Cambridge university press Cambridge; 1995.
- [20] Kresse G, Hafner J. Ab initio molecular dynamics for liquid metals. Phys Rev B. 1993;47:558–561.
- [21] Kresse G. Ab initio molecular dynamics for liquid metals. J Non-Cryst Solids. 1995;192–193:222–229.
- [22] Kresse G, Furthmüller J. Efficient iterative schemes for ab initio total-energy calculations using a plane-wave basis set. Phys Rev B. 1996;54:11169–11186.
- [23] Perdew JP, Burke K, Ernzerhof M. Generalized Gradient Approximation Made Simple. Phys Rev Lett. 1996;77:3865–3868.
- [24] Grimme S. Semiempirical GGA-type density functional constructed with a long-range dispersion correction. J Comput Chem. 2006;27:1787–1799.
- [25] Grimme S, Antony J, Ehrlich S, et al. A consistent and accurate ab initio parametrization of density functional dispersion correction (DFT-D) for the 94 elements H-Pu. J Chem Phys. 2010;132.
- [26] Frenkel D, Smit B. Understanding Molecular Simulation: From Algorithms to Applications. Elsevier; 2023.
- [27] Groß A. Ab initio molecular dynamics simulations of the O2/Pt(111) interaction. Catal Today. 2016;260:60–65.
- [28] Groß A. Hot atom chemistry: Oxygen at stepped platinum surfaces. Appl Surf Sci Adv. 2022;9:100240.
- [29] Kelly E, Seth M, Ziegler T. Calculation of Free Energy Profiles for Elementary Bimolecular Reactions by ab Initio Molecular Dynamics: Sampling Methods and Thermostat Considerations. J Phys Chem A. 2004;108:2167–2180.
- [30] (IUCr) VESTA: a three-dimensional visualization system for electronic and structural analysis [Internet]. [cited 2024 Jan 21]. Available from: https://onlinelibrary.wiley.com/iucr/doi/10.1107/S0021889808012016?casa_token=_hm5LOEWPAAAAA%3ADUwdqLUfeyTNsIwgRSAzqw3UDKVL_F-nL7bJJAKXS-FLyZ6EMv-kNIubFeG7YaQJf0exCLK6IQRm7oc.
- [31] Stukowski A. Visualization and analysis of atomistic simulation data with OVITO—the Open Visualization Tool. Model Simul Mater Sci Eng. 2010;18:015012.
- [32] Dove, Martin, T. Introduction to lattice dynamics (No. 4). Cambridge university press; 1993.

- [33] Pan R, Wang LL, Shanks R, et al. The Influence of Trisilanolisobutyl POSS on Domain Microstructure of a Polyurethane Hybrid Composite: A Molecular Simulation Approach. Silicon. 2019;11:2253–2260.
- [34] Gao X, Liu H, Wei H, et al. Effect of incompletely condensed tri-silanol-phenyl-POSS on the thermal stability of silicone rubber. Polym Bull. 2019;76:2835–2850.
- [35] Yang Wu, Xu Y, Yu J, et al. Enhanced Thermal, Optical and Mechanical Performance of Copolyimide Composite Film Filled with TSP-POSS. Polym Sci Ser B. 2023;65:230–237.
- [36] Leach AR. Molecular Modelling: Principles and Applications. Pearson education; 2001.
- [37] Sutton AP. Electronic structure of materials. Oxford: Clarendon; 2004.
- [38] Choudhuri D, Srinivasan SG, Gibson MA, et al. Exceptional increase in the creep life of magnesium rare-earth alloys due to localized bond stiffening. Nat Commun [Internet]. 2017 [cited 2018 Aug 27];8. Available from: http://www.nature.com/articles/s41467-017-02112-z.
- [39] Choudhuri D. Local structure and bonding environment of intermetallic β1 precipitate phase nucleus in binary Mg-Nd. Comput Mater Sci. 2021;187:110111.
- [40] Tang W, Sanville E, Henkelman G. A grid-based Bader analysis algorithm without lattice bias. J Phys Condens Matter. 2009;21:084204.
- [41] Sanville E, Kenny SD, Smith R, et al. Improved grid-based algorithm for Bader charge allocation. J Comput Chem. 2007;28:899–908.
- [42] Henkelman G, Arnaldsson A, Jónsson H. A fast and robust algorithm for Bader decomposition of charge density. Comput Mater Sci. 2006;36:354–360.
- [43] Choudhuri D, Zheng Y, Alam T, et al. Coupled experimental and computational investigation of omega phase evolution in a high misfit titanium-vanadium alloy. Acta Mater. 2017;130:215–228.
- [44] Alexander S, McTague J. Should All Crystals Be bcc? Landau Theory of Solidification and Crystal Nucleation. Phys Rev Lett. 1978;41:702–705.
- [45] Provatas N, Elder K. Phase-field methods in materials science and engineering. John Wiley & Sons; 2011.
- [46] Abbaschian R, Reed-Hill RE. Physical metallurgy principles-SI version. Cengage Learning; 2009.
- [47] Porter DA, Easterling KE, Sherif MY. Phase transformations in metals and alloys. Boca Raton, FL: CRC Press; 2009.